geet Green Energy and Environmental Technology

IntechOpen Journals

RESEARCH PAPER

Design and Simulations of Solar-Based Hydrogen Production System via Methane Decomposition

Ali R. Al Shehhi[1,2], Ibrahim M. Gadala[3,*] and Mohamed S. Gadala[1]

1 Mechanical Engineering Department, Abu Dhabi University, Abu Dhabi, UAE
2 ADNOC Refining, Abu Dhabi, UAE
3 Materials Engineering Department, The University of British Columbia, Vancouver, BC, Canada
*Corresponding author. E-mail: ibrahimg@interchange.ubc.ca

Citation
Ali R. Al Shehhi, Ibrahim M. Gadala, Mohamed S. Gadala (2024), Design and Simulations of Solar-Based Hydrogen Production System via Methane Decomposition. *Green Energy and Environmental Technology* 3(1), 1–20.

DOI
https://doi.org/10.5772/geet.26

Received: 2 June 2023
Accepted: 22 March 2024
Published: 4 June 2024

Abstract

A solar-based hydrogen production system is analyzed and studied with the intention of optimizing the parameters involved in oil refining industry and the environment of the United Arab Emirates. Methane decomposition in molten salt media using a concentrated solar power system was adopted, since the temperature range required in the system design is achievable with this method. The System Advisor Model software was used in this study with three cases to optimize the system using the levelized cost of heat concept. In Case 1, a levelized cost of heat of 9.32 ¢/kWh was achieved using an optimized system with a CSP-RTUVR-2014 receiver and a Luz LS-3 collector. The design of Cases 1 and 2 exhibited pressure drops along the system of just 10 bar, significantly lower than the 50 bar of Case 3. Similarly, designs of Cases 1 and 2 resulted in maximum receiver thermal losses of around 7 MW, whereas Case 3 yielded 14 MW loss. Analysis of the best-suited molten salt option showed that HITEC solar salt was better than HITEC XL and standard HITEC. A regression analysis was carried out to examine the pressure drop responses since it is a key variable affecting the integrity of the solar system. It was observed that the receiver mass flow rate is the main contributing cause of pressure drop. Through careful operator control of receiver mass flow rate, premature failures of the solar system caused by the pressure drop can be avoided.

Keywords: hydrogen production, catalytic methane decomposition, concentrated solar power, process simulation, levelized cost of heat, molten salt

1. Introduction

In crude oil refining, hydrogen gas is an essential stream in various applications. Many refineries use hydrogen gas in removing sulphur, ammonia and other contaminants from crude oil. Hydro-treating units mainly use hydrogen gas in desulfurization and reducing the emissions of sulphur oxides. Studies on the global breakdown of hydrogen applications indicate that oil refining comprises approximately 30% of hydrogen use in the last 10 years [1]. For these reasons, many refineries have a special hydrogen manufacturing unit (HMU) which requires a catalyst to speed up the chemical reaction of hydrogen production, ensuring lower energy use. The catalyst itself is not consumed in the reactions but needs to be replaced once its life is expended due to its deactivation.

There exist several processes for hydrogen production. They differ in terms of energy source used, feedstock type, and process type. Different routes for hydrogen production are listed below:

- Reforming of hydrocarbon
- Gasification of carbonaceous feedstock
- Decomposition of hydrocarbon
- Thermolysis of Water
- Electrolysis of Water
- Photolysis
- Microbial Electrolysis
- Dark Fermentation

Until recently, the common method to produce hydrogen was steam methane reforming (SMR) [2]. In the United States, more than 95% of the hydrogen is produced by SMR with an annual hydrogen production of 10 million metric tons. Temperature requirements for the SMR process ranges between 700 and 1000 °C with a pressure range of 3–25 bar. The SMR process suffers from several disadvantages, such as high energy consumption and production cost, harsh reaction conditions, low reaction efficiency, and low process stability. More effective methods such as dry reforming of methane (DRM) and partial oxidation of methane (POM) are currently being developed [3]. The above methods generate carbon oxides (COx) as a by-product, which is undesirable and requires a separate expensive process for removal. Therefore, catalytic methane decomposition (CMD) is a preferred alternative to produce hydrogen. Additionally, as indicated above, to decompose methane through direct pyrolysis, a temperature of 1200 °C is required. If the CMD method is used, however, a reasonable yield can be obtained with a much lower temperature. Also, carbon, a by-product generated from CMD, is cheaper than COx by-products and can be separated for secondary use by other industries [4]. In the present work, hydrogen gas is produced from a natural gas (mainly methane gas, CH_4) feed through a CMD process heated by collected solar energy. This work targets the decarbonization of hydrocarbon refining globally but is specifically designed for UAE environment. Implementations of this work can strongly support the shifting of crude oil refining towards clean energy by using a solar-based hydrogen production system which then can be integrated with other downstream applications.

2. *Methane decomposition via solar energy*

2.1. System and collector types

For solar-based hydrogen production systems, Dincer and Joshi [5] classified them into four types: photovoltaic, thermal energy, photo-electrolysis, and bio-photolysis. The temperature requirement of methane pyrolysis processes may be divided into three categories. The most common one a lower temperature (500–700 °C) thermochemical path in presence of a catalyst (catalytic decomposition) [5–7]. However other pathways such as thermal decomposition at higher temperatures (1200 °C) and thermal plasma decomposition at much higher temperatures (e.g., >2000 °C for plasma torch in plasma-assisted reforming of methane (PARM)) are also being considered [8].

In the thermal energy-based hydrogen production systems, different solar collector types can be used with varying operating temperatures, concentration factors, and respective power capacities. Solar collector types like flat plate, vacuum-tube, concentrating trough, field mirror, and parabolic were elucidated and then modified by Dincer and Joshi [5]. It was demonstrated that the concentrating solar trough type has a concentration factor ranging from 40–80 with an operating temperature <350 °C compared to a concentration factor of only 1 for flat plate collector with an operating temperature <200 °C. Methane cracking requires a temperature exceeding 1200 °C to break the strong C–H bonds of methane molecules [9].

2.2. Yield and economics

Laboratory-scale reactions with solar concentrators were carried out by Abanades and Flamant [10] to examine the decomposition of methane. They found that a nearly complete conversion of CH_4 with a hydrogen yield of about 90% can be achieved. Meanwhile, Abbas and Daud [2] posited that the utilization of ethane versus methane results in an increase of hydrogen production at low temperatures and pressures. Additionally, they found that the addition of a noble gas such as Argon increases the yield of hydrogen at high pressures. In methane pyrolysis experiments conducted by Geißler *et al.* [11], increasing liquid metal temperatures resulted in increased hydrogen yields, leading to a maximum hydrogen yield of 78% at 1175 °C.

To make solar-based hydrogen production systems commercial and cost effective, Rodat *et al.* [12] suggested the integration of a carbon sequestration unit. Their economic evaluation showed that the hydrogen production cost can be competitive versus conventional SMR if the carbon black generated is sold. Dincer and Joshi [5] posited that photo-catalytic solar-based water splitting is the most economical and sustainable technology because hydrogen can be obtained directly from abundant and renewable water and sunlight. However, the water used for splitting hydrogen and oxygen often requires treatment and/or desalination, the cost of which was not considered.

2.3. Catalytic methane decomposition (CMD)

Methane gas is decomposed as per Equation (1) below:

$$CH_4 \leftrightarrow C + 2H_2 \tag{1}$$

$$\Delta H = 75.6\ \text{kJ/mol} \tag{2}$$

where ΔH is the essential activation energy to break the firm C–H bonds of methane molecules. Uncatalyzed methane pyrolysis requires a temperature exceeding 1200 °C to break the strong C–H bonds of methane molecules [9]. This very high temperature involves operational and material degradation or integrity challenges. Requiring materials capable of operating at temperatures in excess of 1200 °C adds to project construction costs. Additionally, operating at such high temperatures necessitates the use of more insulation and refractory materials, further adding to costs.

Using catalysts in methane pyrolysis results in significantly lower temperature (500–700 °C) requirements, making them advantageous from the operational, integrity, and cost perspectives. Recently, Gamal *et al.* [13] thoroughly discussed catalyst types which can be used for methane cracking including Co-, Fe-, Ni-, Cu-, and C-based catalysts, in addition to self-standing catalysts. There is no consensus in the literature on the best catalyst for production of H_2 using CMD. The use of commercial Ni catalysts is quite common, though it suffers from the possibility of causing coking issues due to the formation, diffusion, and dissolution of C in Ni-alloys. Other alloys containing elements such as Ru, Rh, Pd, Ir, and Pt yield much

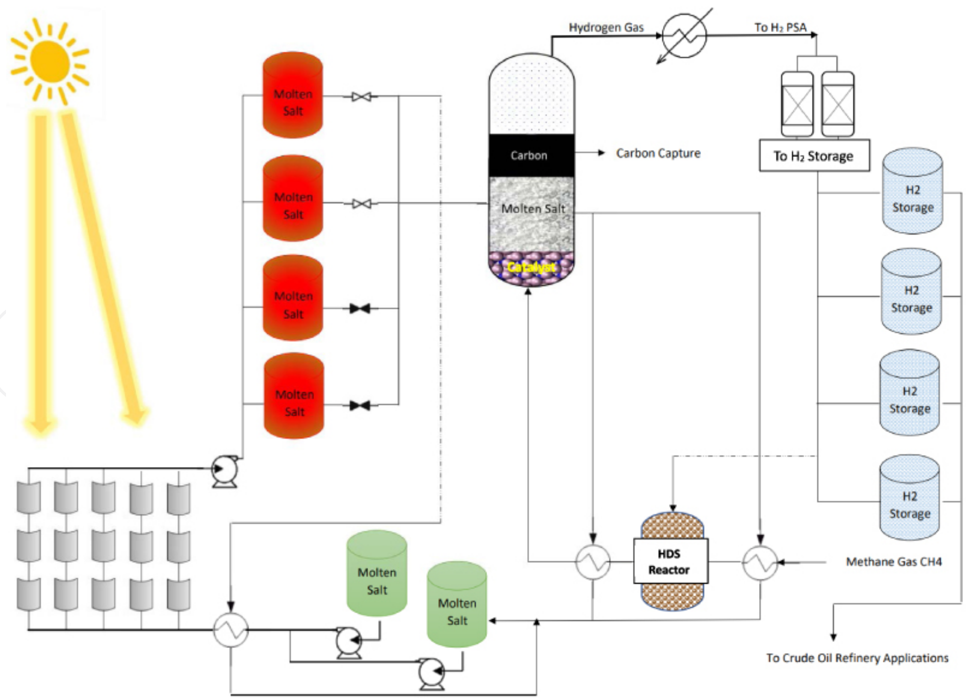

Figure 1. Process flow diagram for solar-based hydrogen production system.

less coking but come at a much higher cost. Fe-based catalysts may quickly oxidize under reaction conditions, whereas Co cannot withstand the higher process pressures. Therefore, for cost, operational, and process factors, Ni-based catalysts were considered for this work. Further discussions of process-induced catalyst breakdown or catalyst-induced degradation of system materials or surfaces is considered beyond the scope of this work.

3. Processes explanation and solar energy collection system

3.1. Process description and flow

The hydrogen production system designed in this work is through a solar-based CMD process. HITEC molten salt was previous characterized for thermal behaviour in solar linear concentrated technologies by Fenandez *et al.* [14], and is a eutectic mixture of water-soluble, inorganic salts of potassium nitrate (53 wt% KNO_3), sodium nitrite (40 wt% $NaNO_2$) and sodium nitrate (7 wt% $NaNO_3$) [15]. It is initially stored in the "cold" tanks, then is transferred to the parabolic trough solar collectors where the solar radiation is captured, increasing its temperature from 270 °C to around 590 °C. There are four storage tanks for the "hot" molten salt, one of which is kept for night-time supply. Molten salt from any of these tanks

Table 1. Selection matrix for different solar energy collection system options.

Criteria	Weighting	Solar energy collection system							
		Parabolic trough		Linear fresnel		Central receiver		Dish/engine	
		Score	Weighted score	Score	Weighted score	Score	Weighted score	Score	Weighted score
Cost of the solar field	0.1	7	0.7	9	0.9	5	0.5	4	0.4
Peak solar efficiency	0.1	7	0.7	5	0.5	6	0.6	9	0.9
Annual solar efficiency	0.15	8	1.2	5	0.75	8	1.2	9	1.35
Concentration ratio	0.1	4	0.4	5	0.5	7	0.7	9	0.9
Construction requirement	0.05	5	0.25	9	0.45	5	0.25	7	0.35
Operating temperature	0.1	7	0.7	7	0.7	10	1	9	0.9
Reliability	0.2	10	2	7	1.4	7	1.4	6	1.2
Land requirement	0.05	5	0.25	9	0.45	5	0.25	7	0.35
Thermal storage	0.15	8	1.2	8	1.2	8	1.2	1	0.15
Total	1		7.4		6.85		7.1		6.5

enters the decomposition reactor at 590 °C. The other feed into the decomposition reactor is methane gas. The Ni-based catalyst filling the reactor allows the decomposition of methane into H_2 and carbon to occur at around 600 °C. The hydrogen gas leaves the reactor from the top where it is then cooled through a series of heat exchangers and sent to a tank farm for temporary storage and subsequent use in refining units on-demand. Figure 1 shows the process flow diagram for solar-based hydrogen production system. It is noted that the system produces carbon as a by-product, which although could be sellable to external users, will not be discussed further in the present work.

3.2. Solar energy collection system selection

A set of 9 selection criteria were considered in a choice matrix. These were: cost of the solar field, peak solar efficiency, annual solar efficiency, concentration ratio, construction requirement, operating temperature, system reliability, land requirement, and thermal storage. Table 1 lists the score of each criterion against the four different solar collection system configurations. A weighting fraction is assigned to each selection criteria. A 0.1 fraction is applied to the scores for the cost of the solar field, peak efficiency, concentration ratio, and operating temperature, since these reasonably contribute to the CMD process. Conversely, land requirement is less significant for refinery sites since they often situated in remote areas such as the desert for UAE. System reliability is a key criterion with a fraction of 0.2, since it is essential to ensure the continuous and reliable production of hydrogen for the refinery. Based on these selection criteria and weights, the parabolic trough solar system was found to be the optimal solar energy collection system for use in the UAE for this work. This choice is supported by related studies by Palenzuela *et al.* [16] on the engineering and economics of concentrating solar power types for desalination plants, which show that the parabolic trough system provides long-term reliability, adequate concentration ratios and operating temperature projections, and appropriate efficiencies, all whilst maintaining reasonable cost.

4. Solar-based hydrogen production system simulations

4.1. Process modelling and simulation

The solar-based hydrogen production system in this work is simulated using the System Advisor Model (SAM) developed by the National Renewable Energy Laboratory (NREL) of the U.S. Department of Energy (DOE) [17]. The modelling process steps in the SAM software began with configuring the location of where the system will be built. In this work, the city of Abu Dhabi in the UAE is chosen, and the solar data was summoned for this location with latitude and longitude of 24.4539 °N and 54.3773 °E, respectively.

Then, the receiver and collector (SCA, solar collector assembly) components were configured. The heat thermal fluid (HTF) was chosen as HITEC molten salt with an operating temperature of 550 °C, required for the CMD process. The factors and parameters considered for selecting HITEC molten salt as the HTF included viscosity, density, heat capacity, and associated pressure loss behaviour. Afterwards, the transport operation limits and loop configuration of the collectors were set up. The number of assemblies per loop is optimizable along with field subsections. The loop thermal efficiency calculation uses the receiver estimated average heat loss, a calculation embedded in the SAM software.

Three cases for SCA makes were studied in this work, as shown in Table 2. Considerations for selecting the collectors included their design weight (low), fasteners requirements, welding or specialized manufacturing requirements, time required for field assembly, extruded parts costs, and mirrors alignment requirements. The values presented by Wagner [18] for HTF factors and parameters were used, and shown in Tables 3, 4, and 5 below.

4.2. Cases and calculations

For the three cases discussed below, the design parameters are driven by the weather library values for the city of Abu Dhabi in the SAM software. The direct normal

Table 2. Receiver and collector make cases used in simulations.

Si no	Receiver make	Collector make
Case 1	Royal Tech CSP RTUVR 2014	Luz LS-3
Case 2	TRX70-125	Solargenix SGX-1
Case 3	Schott PTR70	Euro Trough ET150

Table 3. Case 1 major simulation data inputs.

Design Point Parameters					
Solar Field			**Heat Sink**		
Design Point DNI	950	W/m²	Heat sink power	28.00	MW
Design Point DNI	2.5		Pumping power for HTF trough heat sink	0.55	KW/KG/S
Target Receiver thermal Power	70.00	MW	Model piping through heat sink?		
Loop inlet HTF temperature	290	°C	Length of Piping through heat sink	50.0	m
Loop outlet HTF temperature	560	°C	Choose Number of Loops	☑	
			Thermal Energy Storage		
			Hours of Storage at design point	14	
System Summary					
Actual number of loops	14		Actual solar multiple	2.53	
Total aperture reflective area	106,820.0	m²	Actual field thermal output	70.72	MW
Solar Field Design Point					
Single loop aperture	7630	m²	Actual number of loops	14	
Loop optical efficiency	0.746		Total aperture reflective area	106,820	m²
Total loop conversion efficiency	0.697		Actual solar multiple	2.53	
Total required aperture, SM=1	42,292	m²	Actual field thermal output	70.7213	MW
Required number of loops, SM=1	6		Loop inlet HTF temperature	290	°C
Total Tracking power	24,500	W	Loop outlet HTF temperature	560	°C
Solar Field Parameters			**Heat Transfer Fluid**		
Row Spacing	15	m	Field HTF fluid	Hitec Solar Salt	
Header pipe roughness	4.57e-05	m	Filed HTF min operating temp	238	°C
HTF Pump efficiency	0.85		Field HTF max operating temp	593	°C
Piping thermal loss coefficient	0.45	W/m²-K	Freeze protection temp	280	°C
Wind stow speed	25	m/s	Min single loop flow rate	1.75	Kg/s
Receiver startup delay time	0.2	Hr	Max single loop flow rate	13.74	Kg/s
Receiver startup delay energy fraction	0.25	-	Min filed flow velocity	0.3	m/s
Collector startup energy	0.021	kWHe/sca	Max filed flow velocity	2.3	m/s
Tracking power per SCA	125	W/sca		Cold Headers / Hot Headers	
Number of filed subsections	8		Header design min flow velocity	2 m/s / 2 m/s	
Allow partial defocusing	Simultaneous	☑	Header design max flow velocity	3 m/s / 3 m/s	
Collector Type					
Collector name from Library	Luz LS-3		Apply Values from Library		
Collector Geometry					
Reflective aperture area	545	m²	Number of modules per assembly	12	
Aperture width, total structure	5.75	m	Average surface-to focus path length	2.11	m
Length of collector assembly	100	m	Piping distance between assembles	1	m
Optical Parameters					
Incidence angle modifier coefficient	N/A		Geometry effects	0.98	
Tracking error	0.99		Mirror reflectance	0.935	
General optical error	0.99	m	Dirt on mirror	0.97	
Optical Calculations					
Length of single module	8.3333	m	End loss at summer solstice	0.999968	
IAM at summer solstice	1.00086		Optical efficiency at design	0.871124	
Receiver Type					
Receiver name from Library	Royal Tech CSP RTUVR 2014 (Manufacturer Specification)		Apply Values from Library		
Receiver Geometry					
Absorber tube inner diameter	0.066	m	Absorber flow plug diameter	0	m
Absorber tube outer diameter	0.07	m	Internal surface roughness	2e-05	
Glass envelope inner diameter	0.119	m	Absorber flow pattern	Tube flow	
Glass envelope outer diameter	0.125		Absorber material type	321H	

irradiation (DNI) parameter, which is the quantity of solar radiation received per unit area of the collector, is considered as 950 W/m². The density of the HTF (i.e., HITEC molten salt) simulated is 1819.7 kg/m³ and operating temperature is 550 °C, adequate for the CMD process. To avoid the freezing of the HTF, the loop inlet temperature parameter is maintained at temperature higher than the HTF freezing

Table 4. Case 2 major simulation data inputs.

Design Point Parameters							
Solar Field			**Heat Sink**				
Design Point DNI	950	W/m²	Heat sink power	28.00	MW		
Design Point DNI	2.5		Pumping power for HTF trough heat sink	0.55	kW/kg/s		
Target Receiver thermal Power	70.00	MW	Model piping through heat sink?				
Loop inlet HTF temperature	290	°C	Length of Piping through heat sink	50.0	m		
Loop outlet HTF temperature	560	°C	Choose Number of Loops		☑		
			Thermal Energy Storage				
			Hours of Storage at design point	14			
System Summary							
Actual number of loops	16		Actual solar multiple	2.50			
Total aperture reflective area	105,347.2	m²	Actual field thermal output	70.12	MW		
Solar Field Design Point							
Single loop aperture	6584	m²	Actual number of loops	16			
Loop optical efficiency	0.758		Total aperture reflective area	105,347	m²		
Total loop conversion efficiency	0.701		Actual solar multiple	2.50			
Total required aperture, SM=1	42,067	m²	Actual field thermal output	70.1201	MW		
Required number of loops, SM=1	7		Loop inlet HTF temperature	290	°C		
Total Tracking power	28,000	W	Loop outlet HTF temperature	560	°C		
Solar Field Parameters			**Heat Transfer Fluid**				
Row Spacing	15	m	Field HTF fluid	Hitec Solar Salt			
Header pipe roughness	4.57e-05	m	Filed HTF min operating temp	238	°C		
HTF Pump efficiency	0.85		Field HTF max operating temp	593	°C		
Piping thermal loss coefficient	0.45	W/m²-K	Freeze protection temp	280	°C		
Wind stow speed	25	m/s	Min single loop flow rate	1.75	Kg/s		
Receiver startup delay time	0.2	Hr	Max single loop flow rate	13.74	Kg/s		
Receiver startup delay energy fraction	0.25	-	Min filed flow velocity	0.3	m/s		
Collector startup energy	0.021	kWHe/sca	Max filed flow velocity	2.3	m/s		
Tracking power per SCA	125	W/sca		Cold Headers		Hot Headers	
Number of filed subsections	8		Header design min flow velocity	2	m/s	2	m/s
Allow partial defocusing	Simultaneous	☑	Header design max flow velocity	3	m/s	3	m/s
Collector Type							
Collector name from Library	Solargenix SGX-1		Apply Values from Library				
Collector Geometry							
Reflective aperture area	470.3	m²	Number of modules per assembly	12			
Aperture width, total structure	5	m	Average surface-to focus path length	1.8	m		
Length of collector assembly	100	m	Piping distance between assembles	1	m		
Optical Parameters							
Incidence angle modifier coefficient	N/A		Geometry effects	0.98			
Tracking error	12		Mirror reflectance	0.935			
General optical error	1.8	m	Dirt on mirror	0.97			
Optical Calculations							
Length of single module	8.3333	m	End loss at summer solstice	0.999973			
IAM at summer solstice	1.00086		Optical efficiency at design	0.874643			
Receiver Type							
Receiver name from Library	Royal Tech CSP RTUVR 2014(Manufacturer Specification)		Apply Values from Library				
Receiver Geometry							
Absorber tube inner diameter	0.066	m	Absorber flow plug diameter	0	m		
Absorber tube outer diameter	0.07	m	Internal surface roughness	4.5e-05			
Glass envelope inner diameter	0.119	m	Absorber flow pattern	Tube flow			
Glass envelope outer diameter	0.125		Absorber material type	216L			

point of 290 °C. Initially, the HTF storage time is set as 14 h. Parallel tank pairs were considered for all cases, each tank with a height of 15 m and a diameter of 9.1 m. Figure 2 illustrates the system design with values for the Case 1 as an example.

4.2.1. Case 1

A summary of all input parameters for Case 1 is shown in Table 3, excluding inputs for the storage system design which are beyond the scope of this paper.

The total loop conversion efficiency for this case is 69.7% with an actual field thermal output of 70.7 MW. The reflective aperture area of the Luz LS-3 collector type in this case is 545 m². The absorber tube inner diameter (D) of the Royal Tech CSP RTUVR 2014 receiver type in this case is 0.066 m.

Table 5. Case 3 major simulation data inputs.

Design Point Parameters

Solar Field			Heat Sink		
Design Point DNI	950	W/m²	Heat sink power	28.00	MW
Design Point DNI	2.5		Pumping power for HTF trough heat sink	0.55	kW/kg/s
Target Receiver thermal Power	70.00	MW	Model piping through heat sink?		
Loop inlet HTF temperature	290	°C	Length of Piping through heat sink	50.0	m
Loop outlet HTF temperature	560	°C	Choose Number of Loops		☑
			Thermal Energy Storage		
			Hours of Storage at design point	14	

System Summary

Actual number of loops	10		Actual solar multiple	2.75	
Total aperture reflective area	114,450	m²	Actual field thermal output	76.97	MW

Solar Field Design Point

Single loop aperture	11,445	m²	Actual number of loops	10	
Loop optical efficiency	0.758		Total aperture reflective area	114.450	m²
Total loop conversion efficiency	0.708		Actual solar multiple	2.75	
Total required aperture, SM=1	41,635	m²	Actual field thermal output	76.9688	MW
Required number of loops, SM=1	4		Loop inlet HTF temperature	290	°C
Total Tracking power	17,500	W	Loop outlet HTF temperature	560	°C

Solar Field Parameters			Heat Transfer Fluid		
Row Spacing	15	m	Field HTF fluid	Hitec Solar Salt	
Header pipe roughness	4.57e-05	m	Filed HTF min operating temp	238	°C
HTF Pump efficiency	0.85		Field HTF max operating temp	593	°C
Piping thermal loss coefficient	0.45	W/m²-K	Freeze protection temp	280	°C
Wind stow speed	25	m/s	Min single loop flow rate	1.75	Kg/s
Receiver startup delay time	0.2	Hr	Max single loop flow rate	13.74	Kg/s
Receiver startup delay energy fraction	0.25	-	Min filed flow velocity	0.3	m/s
Collector startup energy	0.021	kWHe/sca	Max filed flow velocity	2.3	m/s
Tracking power per SCA	125	W/sca		Cold Headers	Hot Headers
Number of filed subsections	8		Header design min flow velocity	2 m/s	2 m/s
Allow partial defocusing	Simultaneous	☑	Header design max flow velocity	3 m/s	3 m/s

Collector Type

Collector name from Library	EuroTrough ET150	Apply Values from Library

Collector Geometry

Reflective aperture area	817.5	m²	Number of modules per assembly	12	
Aperture width, total structure	5.75	m	Average surface-to focus path length	2.11	m
Length of collector assembly	150	m	Piping distance between assembles	1	m

Optical Parameters

Incidence angle modifier coefficient	N/A		Geometry effects	0.98	
Tracking error	0.99		Mirror reflectance	0.935	
General optical error	0.99	m	Dirt on mirror	0.97	

Optical Calculations

Length of single module	8.3333	m	End loss at summer solstice	0.999968	
IAM at summer solstice	1.00086		Optical efficiency at design	0.871124	

Receiver Type

Receiver name from Library	Royal Tech CSP RTUVR 2014(Manufacturer Specification)	Apply Values from Library

Receiver Geometry

Absorber tube inner diameter	0.066	m	Absorber flow plug diameter	0	m
Absorber tube outer diameter	0.07	m	Internal surface roughness	4.5e-05	
Glass envelope inner diameter	0.115	m	Absorber flow pattern	Tube flow	
Glass envelope outer diameter	0.12		Absorber material type	304L	

Initially, a reference pressure loss is considered as baseline for the study. By using the Therminol-VP1 settings identified in the SAM software in terms of its properties like velocity, density (ρ), and dynamic viscosity (μ), the HTF is altered to obtain the new configuration designed and compare the outputs. A maximum Therminol-VP1 velocity of V_t = 5 m/s is used. The Reynolds Number (Re_T) is then calculated as per Equations (3) and (4) below:

$$Re = \frac{\rho V_t D}{\mu} \tag{3}$$

$$Re_T = \frac{773\ \frac{\text{kg}}{\text{m}^3} * 5\ \frac{\text{m}}{\text{s}} * 0.066\ \text{m}}{0.185\text{E-}3} = 1.38\text{E}6 \tag{4}$$

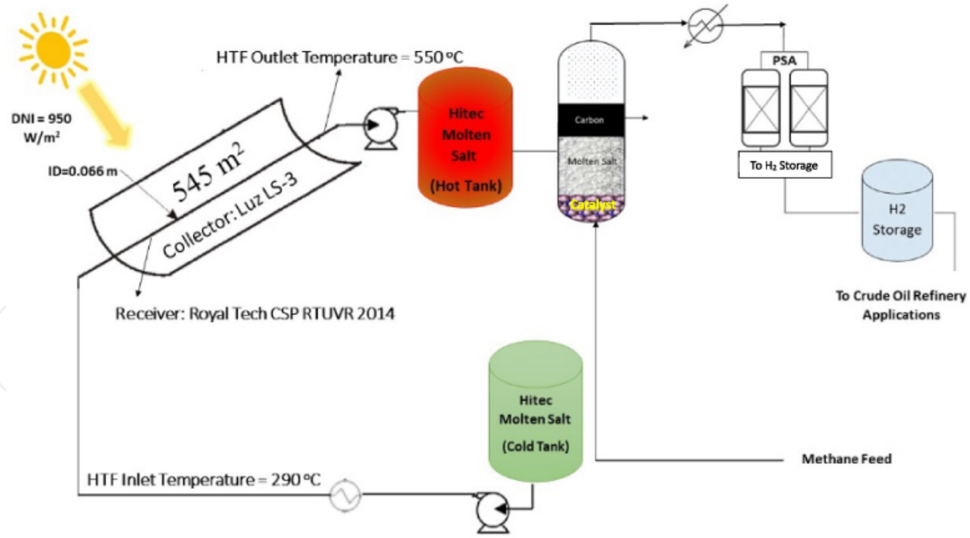

Figure 2. Schematic of system design for Case 1 as an example.

A friction factor (f_F) of 0.012 at Re_T and a Relative Pipe Roughness (RPR) on the order of 10E-4 (assumed) was obtained from a standard Moody Chart. The initial reference length (l_{ref}) was set as 1.0 m. Solving for pressure loss using Equation (5) yields a value of 1.76E3 kg/cm² which is then matched to the reference pressure constant using the salt loop mass flow rates described below.

$$\Delta P_{\text{ref}} = f_F(Re_T)\frac{\rho_T V_T^2 l_{\text{ref}}}{2D}. \tag{5}$$

An energy ($\dot{q}_{\text{loop}}$) balance is used to calculate the molten salt mass flow rate ($\dot{m}_s$), where the absorption energy of Equation (6) is equated to the first law energy balance of Equation (7). The $\dot{m}_s$ can then be written as Equation (8).

$$\dot{q}_{\text{loop}} = A_{\text{sca}}\eta_{\text{abs}}N_{\text{sca}}I_{bn} \tag{6}$$

$$\dot{q}_{\text{loop}} = \dot{m}_s C_{ps}\Delta T_s \tag{7}$$

$$\dot{m}_s = \frac{A_{\text{sca}}\eta_{\text{abs}}N_{\text{sca}}I_{bn}}{C_{ps}\Delta T_s}. \tag{8}$$

The values used for the parameters in Equations (6)–(8) yielding a $\dot{m}_s$ of 6.9 kg/s are as follows.

$$A_{sca} = 545 \text{ m}^2 \tag{9}$$

$$\eta_{abs} = 0.697 \tag{10}$$

$$I_{bn} = 950 \text{ w/m}^2 \tag{11}$$

$$C_{ps} = 1520 \text{ J/kg K} \tag{12}$$

$$\Delta T_s = 560 - 290 = 270\ ^\circ\text{C} \tag{13}$$

$$N_{sca} = 8 \text{ (initial estimate)}. \tag{14}$$

Calculating molten salt velocity (V_s) from $\dot{m}_s$ follows Equation (15), yielding 1.1 m/s. The Reynolds Number for the molten salt (Re_s) is computed as before using Equation (3), yielding a value of 8.29E4. A f_{FT} of 0.019 at the Re_s and the same RPR as before was again found from a standard Moody Chart.

$$V_s = \frac{\dot{m}_s}{\rho_s \pi (\frac{D}{2})^2}. \tag{15}$$

The pressure drop equation can then be solved for the actual length (l'), as per Equation (16). This yields an actual value of 5.6 m for the first iteration, versus l_{ref} which was initially set to 1.0 m. Similarly, using the l' actual, the number of collectors or SCAs (N'_{sca}) can by recomputed. For the first iteration, this recalculation yields a value of 16, versus N_{sca} which was initially set as 8.

$$l' = \frac{\Delta P_{ref} 2D}{\rho_s V_s^2 f_{fs}}. \tag{16}$$

The calculation steps outlined above were iterated with multiple initial estimates for l_{ref} and N_{sca}, keeping $A_{sca} = 545 \text{ m}^2$ and $\eta_{abs} = 0.697$ for this collector-receiver type in Case 1. The values converge to a $l' = 1.64$ m and a $N'_{sca} = 14$ used for this simulation of this case.

4.2.2. Case 2

A summary of all input parameters for Case 2 is shown in Table 4, excluding inputs for the storage system design which are beyond the scope of this paper.

The total loop conversion efficiency for this case is 70.1% with an actual field thermal output of 70.12 MW. The reflective aperture area of the Solargenix SGX-1 collector type in this case is 470 m². The absorber tube inner diameter of the TRX70-125 receiver type in this case remains as 0.066 m (unchanged from Case 1).

Again, the same methodology covered in Equations (1)–(8) from Case 1 was deployed here, except using $A_{sca} = 470 \text{ m}^2$ and $\eta_{abs} = 0.701$ instead. With this change, the following updated results for V_s, $Re_s, f(Re_s)$, l', and N'_{sca} were found.

$$V_s = 0.981 \text{ m/s} \tag{17}$$

$$Re_s = 7.36\text{E}4 \tag{18}$$

$$f(Re_s) = 0.018 \tag{19}$$

$$l' = 1.95 \text{ m} \tag{20}$$

$$N'_{\text{sca}} = 16 \tag{21}$$

4.2.3. Case 3

A summary of all input parameters for Case 3 is shown in Table 5, excluding inputs for the storage system design which are beyond the scope of this paper.

The total loop conversion efficiency for this case is 70.8% with an actual field thermal output of 77 MW. The reflective aperture area of the EuroTrough ET150 collector type in this case is 818 m². The absorber tube inner diameter of the Schott PTR70 receiver type in this case remains as 0.066 m (unchanged from Cases 1 and 2).

Once again, the same methodology covered in Equations (1)–(8) from Case 1 was deployed here, except using A_{sca} = 818 m² and η_{abs} = 0.708 instead. With this change, the following updated results for V_s, $Re_s, f(Re_s)$, l', and N'_{sca} were found.

$$V_s = 0.861 \text{ m/s} \tag{22}$$

$$Re_s = 6.46\text{E}4 \tag{23}$$

$$f(Re_s) = 0.020 \tag{24}$$

$$l' = 8.812 \text{ m} \tag{25}$$

$$N'_{\text{sca}} = 16. \tag{26}$$

5. Simulation outputs and analysis

5.1. Simulation outputs

In this section, the results from the SAM software for the three cases are presented and discussed. Based on the inputs described in the previous sections, Figure 3 shows the annual net energy, annual gross energy, annual thermal freeze protection requirement, and annual electricity load for the three cases considered in this work. As seen in this figure, the annual net energy (kWh) for Case 1 is the highest, followed by Case 2 and then Case 3. Notably, in Case 2 although the annual gross energy (kWh) is higher than in Case 1, the thermal freeze protection requirements are also higher, making the annual net energy lower than Case 1. The levelized cost

Figure 3. Comparisons of simulations results between the three cases considered.

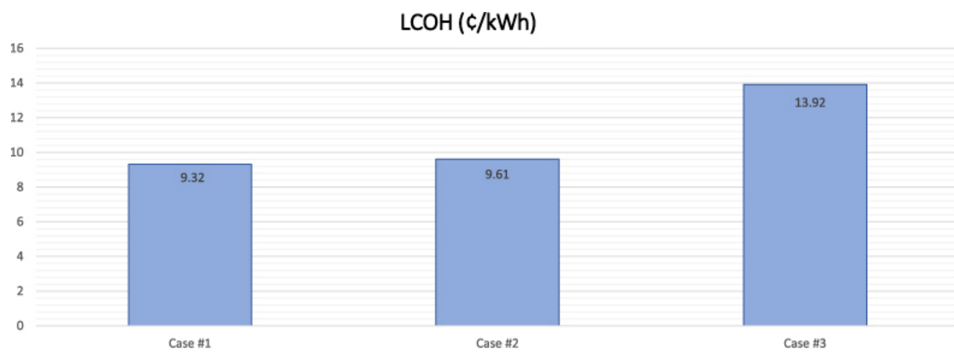

Figure 4. LCOH results of the three cases considered.

of heat (LCOH) for the three cases considered in this work is shown in Figure 4. As seen in Figure 4, the LCOH is lowest for Case 1 at around 9.32 ¢/kWh. When evaluated on an annual profile, field protection requirements for the three cases were expectedly higher at the beginning of the year due to the winter condition in the UAE. Then, as the summer season commences, the field freeze protection requirement starts reducing for all three cases. Case 1 exhibits the minimum freeze protection requirement among the three cases, which makes it the optimum choice in terms of LCOH.

Simulation outputs for three of the most important parameters, namely field pressure drop, receiver thermal losses, and field protection (from molten salt freezing) requirements are discussed here. Figure 5 illustrates the field pressure drop in bar for the three cases studied. The profile increases in the summer to around 10 bar. The profile for Case 2 exhibits a nearly identical fashion and very similar values to that of Case 1. However, for Case 3 shown in Figure 5, the pressure drop soared to

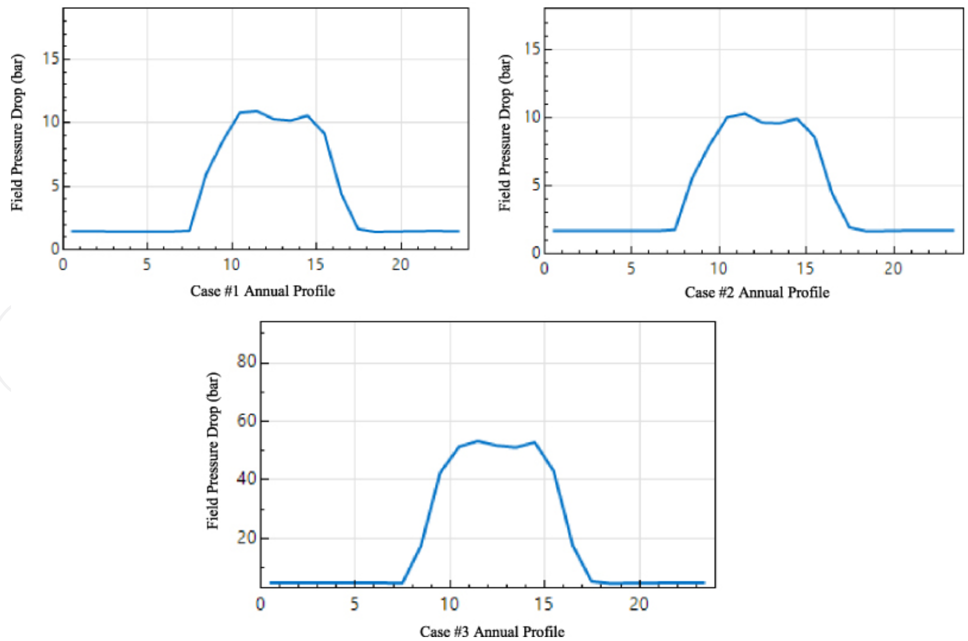

Figure 5. Field pressure drop results of Cases 1, 2, and 3.

about 50 bar around halfway through the year. The same significant difference between the first two cases and Case 3 is observed for the receiver thermal losses parameter (MW), shown in Figure 6. As seen in Figure 6, the receiver thermal losses for Case 1 records a maximum of nearly 7 MW in the annual profile obtained from the SAM software for the city of Abu Dhabi. A similar behaviour and nearly identical values are exhibited in Case 2. Contrastingly, the receiver thermal losses in Case 3 reached double that of Cases 1 and 2, at around 14 MW.

As shown in Figure 7, the field protection (from molten salt freezing) requirement for the three cases are expectedly higher at the beginning of the year due to winter condition in the UAE. They peak at values between 2 and 3 MW for all three cases. Then, for all three cases, as summer season commences, the field freeze protection requirements start reducing. Case 1 exhibits the minimum freeze protection requirement among the three cases, which translates to the lowest cost requirement for continued operation throughout the year.

The influence of molten salt type (HITEC models) on the LCOH was also studied. By maintaining the configuration of the Case 1 in terms of collector and receiver types, the HTF type was the adjustment variable. The control HTF studied was HITEC solar salt (specific to CSP applications) with maximum operating temperature capabilities of about 593 °C. This was compared to HITEC XL with a maximum operating temperature of around 500 °C and HITEC standard with a maximum operating temperature up to 538 °C. Based on the LCOH obtained for the

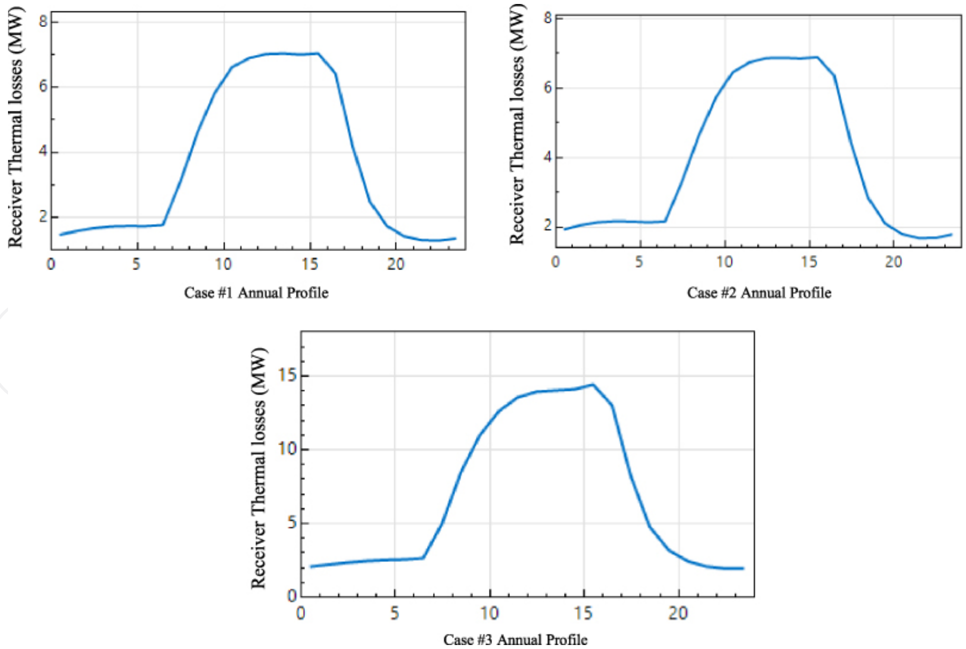

Figure 6. Receiver thermal losses results of Cases 1, 2, and 3.

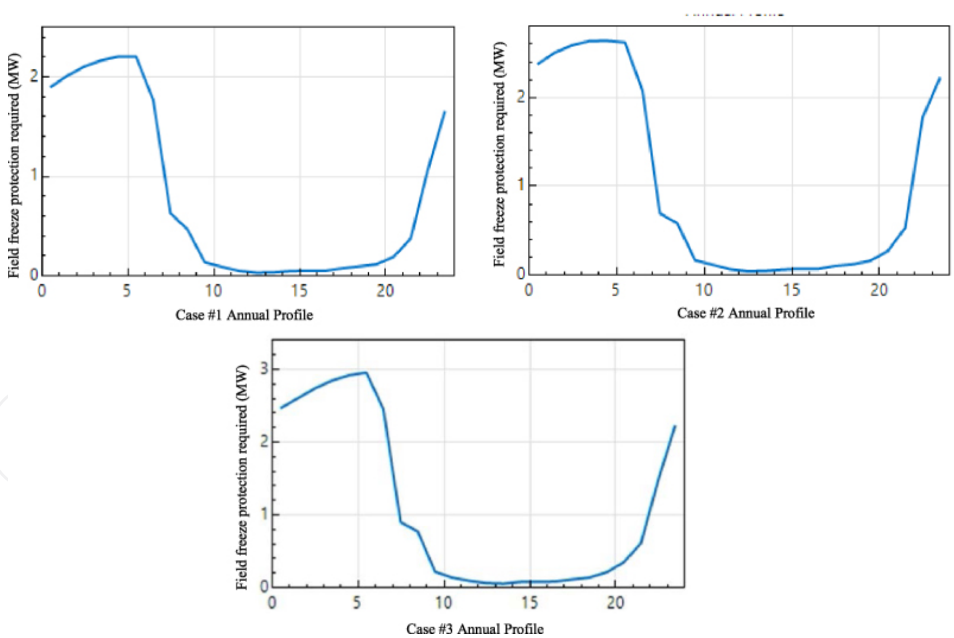

Figure 7. Field protection (from molten salt freezing) results of Cases 1, 2, and 3.

three HTF cases, shown in Figure 8, the control case (i.e., HITEC solar salt used throughout this paper) maintained its superiority over the HITEC XL and HITEC standard counterparts based on the highest operating temperature to LCOH

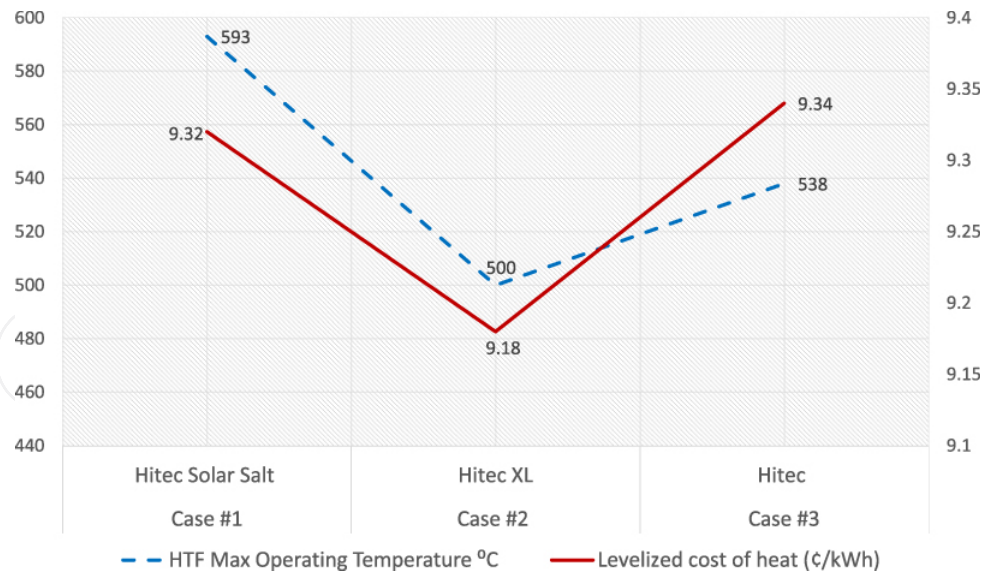

Figure 8. HTF simulation results for HITEC solar salt, XL, and standard variants.

(T:LCOH) ratio. Although the LCOH for the HITEC XL is lower than HITEC solar salt, its maximum operating temperature of 500 °C is too low to sustain the CMD process at profitable yields. Furthermore, the T:LCOH ratio of HITEC XL is only 54, compared to 64 for HITEC solar salt.

5.2. Regression analysis

Since the pressure drop is one of the main variables affecting the integrity of the solar-based hydrogen production system, it is essential to understand which operating or design variables affect it. Also, the behaviour of pressure drop versus these variables needs to be characterized. To address this concern, a regression analysis was carried out using Minitab to examine the pressure drop response. Initially, ten variables were identified for the regression analysis, namely: field thermal power incident, field averaged outlet temperature, field total mass flow delivered, receiver mass flow rate, receiver thermal losses, receiver thermal power incident, TES (thermal energy storage) freeze protection power, TES thermal losses, resource beam normal irradiance, and resource dry bulb temperature. These variables are denoted x_1 through x_{10} in the regression Equation (27). These independent variables influence the output variable (also known as the response variable), namely the pressure drop in this analysis which is denoted y in Equation (27). These ten variables are accepted or rejected based on the p-value generated from the regression analysis, with a 5% significance screening indicator,

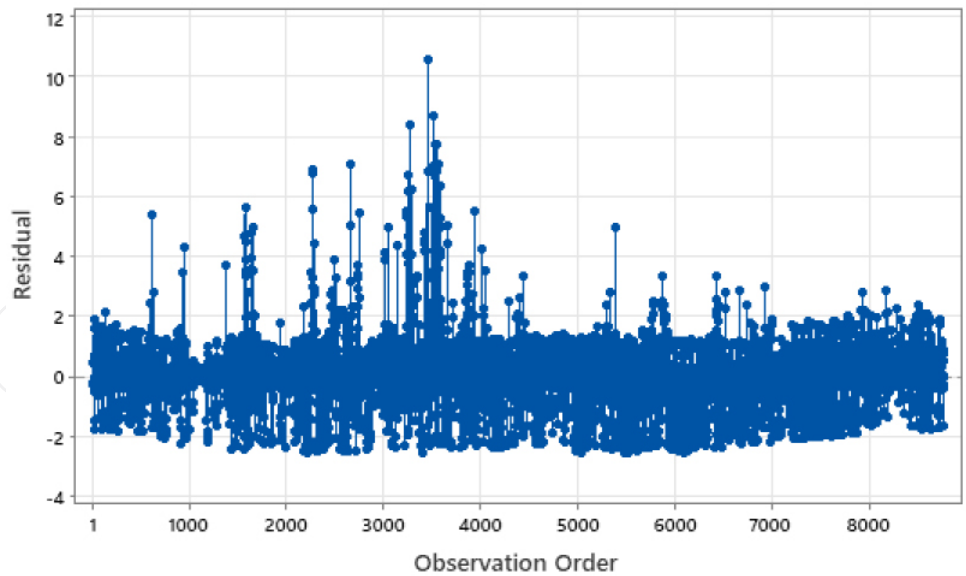

Figure 9. Data point observation order vs. residuals for pressure drop (response variable).

or $\alpha = 0.05$.

$$y = -2.8699 + 0.33\,x_1 - 0.002124\,x_2 + 0.01882\,x_3 + 3.0766\,x_4 - 0.2273\,x_5 + 0.07666\,x_6 + 0.54\,x_7 + 1.330\,x_8 - 0.040\,x_9 - 0.01438\,x_{10}. \tag{27}$$

The regression equation was obtained with the ten variables for the response of the pressure drop. A total of 8760 data points were considered in this analysis based on the hourly data for each variable. As shown in Figure 9, the majority of data points were within ±2 residuals for the output variable (i.e., pressure drop). Three input variables were rejected as a result of the analysis, namely field thermal power incident, TES freeze protection power, and resource beam normal irradiance, with p-values 0.877, 0.867, and 0.862, respectively. Eventually, only seven variables are considered acceptable as affecting the pressure drop response. However, of these, only the receiver mass flow rate could be considered as a main contributing variable towards the pressure drop behaviour. This is based on the R^2-value for this variable being >95%, the rest were <75%. By knowing that the mass flow rate is the main parameter affecting pressure drop, the operator of the system can better control adjustable system inputs to delay or avoid failures of this solar-based hydrogen production system.

6. Conclusion(s)

The key objective of this work was to establish a basis and assessment for solar-based hydrogen production in the UAE. Although principles applied in this work are intended for oil and gas refining, they are extendable to other industries. In the suggested catalytic methane decomposition (CMD) process heated using collected solar energy, carbon dioxide emissions are only 0.05 mol CO_2 per mol of hydrogen produced, which is much smaller than the 0.43 mol of CO_2 per mol of hydrogen produced with the current unit in the subject refinery.

Based on the several simulations, the first collector and receiver components of the Case 1 was found to be the most promising. The System Advisor Model (SAM) software was used for simulation of the system using the concentrating parabolic trough—heat model. With a total loop conversion efficiency for Case 1, 2, and 3 of 69.7%, 70.1%, and 70.8% respectively, the levelized cost of heat (LCOH) for the three cases with their different design inputs parameters placed Case 1 at the lowest cost. This optimized system (Case 1) can be achieved with a LCOH of 9.32 ¢/kWh by using a CSP-RTUVR-2014 receiver and a Luz LS-3 collector. This design results in the minimum freeze protection requirement of the three designs studied. Also, the design of Case 1 exhibits a pressure drop along the system of only 10 bar, similar to Case 2 but significantly lower than the 50 bar of Case 3. Ten variables were analysed using regression to understand which ones affect the critical parameter of pressure drop. Eventually, only seven variables were considered acceptable to affect the pressure drop response, and ultimately only the receiver mass flow rate could be considered as a main contributing variable towards the pressure drop behaviour. Finally, in analysing the influence of molten salt types on the LCOH, where the configuration of the Case 1 collector and receiver types was maintained, it was found that HITEC solar salt is the best option versus HITEC XL and standard HITEC.

Conflict of interest

The authors declare no conflict of interest.

Acknowledgements

The authors acknowledge the support of Abu Dhabi National Oil Company (ADNOC) Refining in conducting this work. The statements made herein are solely the responsibility of the authors.

References

1 Gielen D, Taibi E, Miranda R. *Hydrogen: a renewable energy perspective*. Abu Dhabi: International Renewable Energy Agency; 2019.

2 Abbas HF, Daud WW. Hydrogen production by methane decomposition: a review. *Int J Hydrogen Energy*. 2010;**35**(3):1160–1190.

3 Kim H, Kim H, Kim S, Lee S, Kim J. Hydrogen production in methane decomposition reactor using solar thermal energy. *Appl Sci*. 2021;**11**(21):10333.

4 Zhang J, Li X, Chen H, Qi M, Zhang G, Hu H, Ma X. Hydrogen production by catalytic methane decomposition: carbon materials as catalysts or catalyst supports. *Int J Hydrogen Energy*. 2017;**42**(31):19755–19775.

5 Dincer I, Joshi AS. *Solar based hydrogen production systems*. Cham: Springer; 2013.

6 Fan Z, Weng W, Zhou J, Gu D, Xiao W. Catalytic decomposition of methane to produce hydrogen: a review. *J Energy Chem*. 2020;**58**: 415–430.

7 Hasnan NSN, Timmiati SN, Lim KL, Yaakob Z, Kamaruddin NHN, Teh LP. Recent developments in methane decomposition over heterogeneous catalysts: an overview. *Mater Renew Sustain Energy*. 2020;**9**(2):1–18.

8 Schneider S, Bajohr S, Graf F, Kolb T. State of the art of hydrogen production via pyrolysis of natural gas. *Chem Bio Eng Rev*. 2020;**7**(5):150–158.

9 Muradov N, Smith F, Huang C, Ali T. Autothermal catalytic pyrolysis of methane as a new route to hydrogen production with reduced CO2 emissions. *Catal Today*. 2006;**116**(3):281–288.

10 Abanades S, Flamant G. *Hydrogen production by the solar thermal decomposition of methane using a high temperature solar chemical reactor*. Miami, FL: IAHE; 2006.

11 Geißler T, Abánades A, Heinzel A. Hydrogen production via methane pyrolysis in a liquid metal bubble column reactor with a packed bed. *Chem Eng J*. 2016;**299**: 192–200.

12 Rodat S, Abanades S, Flamant G. Co-production of hydrogen and carbon black from solar thermal methane splitting in a tubular reactor prototype. *Solar Energy*. 2011;**85**(4):645–652.

13 Gamal A, Eid K, El-Naas MH, Kumar D, Kumar A. Catalytic methane decomposition to carbon nanostructures and COx-free hydrogen: a mini-review. *Nanomaterials [Internet]*. 2021 May 6;**11**(5):1226.

14 Fernández AG, Galleguillos H, Fuentealba E, Pérez FJ. Thermal characterization of HITEC molten salt for energy storage in solar linear concentrated technology. *J Therm Anal Calorim*. 2015;**122**: 3–9.

15 Zou L, Chen X, Wu Y, Pérez FJ. Experimental study of thermophysical properties and thermal stability of quaternary nitrate molten salts for thermal energy storage. *Solar Energy Mater Solar Cells*. 2019;**190**: 12–19.

16 Palenzuela P, Alarcón-Padilla DC, Zaragoza G. *Concentrating solar power and desalination plants: engineering and economics of coupling multi-effect distillation and solar plants*. Cham: Springer; 2015.

17 System Advisor Model Version 2020.11.29 (SAM 2020.11.29). National Renewable Energy Laboratory. Golden, CO [Internet]; 2021 [Accessed December 22]. Available from: https://sam.nrel.gov.

18 Wagner M. Modeling parabolic trough systems. 2014. Retrieved from https://sam.nrel.gov.